Fabrication of Carbon-Based Hydrogel Membrane for Landfill Leachate wastewater treatment

Elika Karbassiyazdi[a], Ali Altaee[a] , Ibrar Ibrar[a], Amir Razmjou[b], Namuun Ganbat[a], Ali Malekizadeh[a], Romina Ghobadi [a], Hadi Khabbaz [a]

[a] Center for Green Technology, School of Civil and Environmental Engineering, University of Technology Sydney, 15 Broadway, NSW 2007, Australia

[b] Mineral Recovery Research Center (MRRC), School of Engineering, Edith Cowan University, Joondalup, Perth, WA, 6027, Australia

*Corresponding author Email address: ali.altaee@uts.edu.au

Highlights:

- A carbon-based hydrogel membrane was fabricated to achieve a high rejection rate and water flux
- Impact of carbon concentrations and centrifugation speeds on ions rejection was evaluated
- The rejection of 4CG hydrogel membrane for divalent ions followed the order Pb>Cu>Mg>Ca
- The 4CG hydrogel membrane demonstrated consistent performance over four consecutive cycles

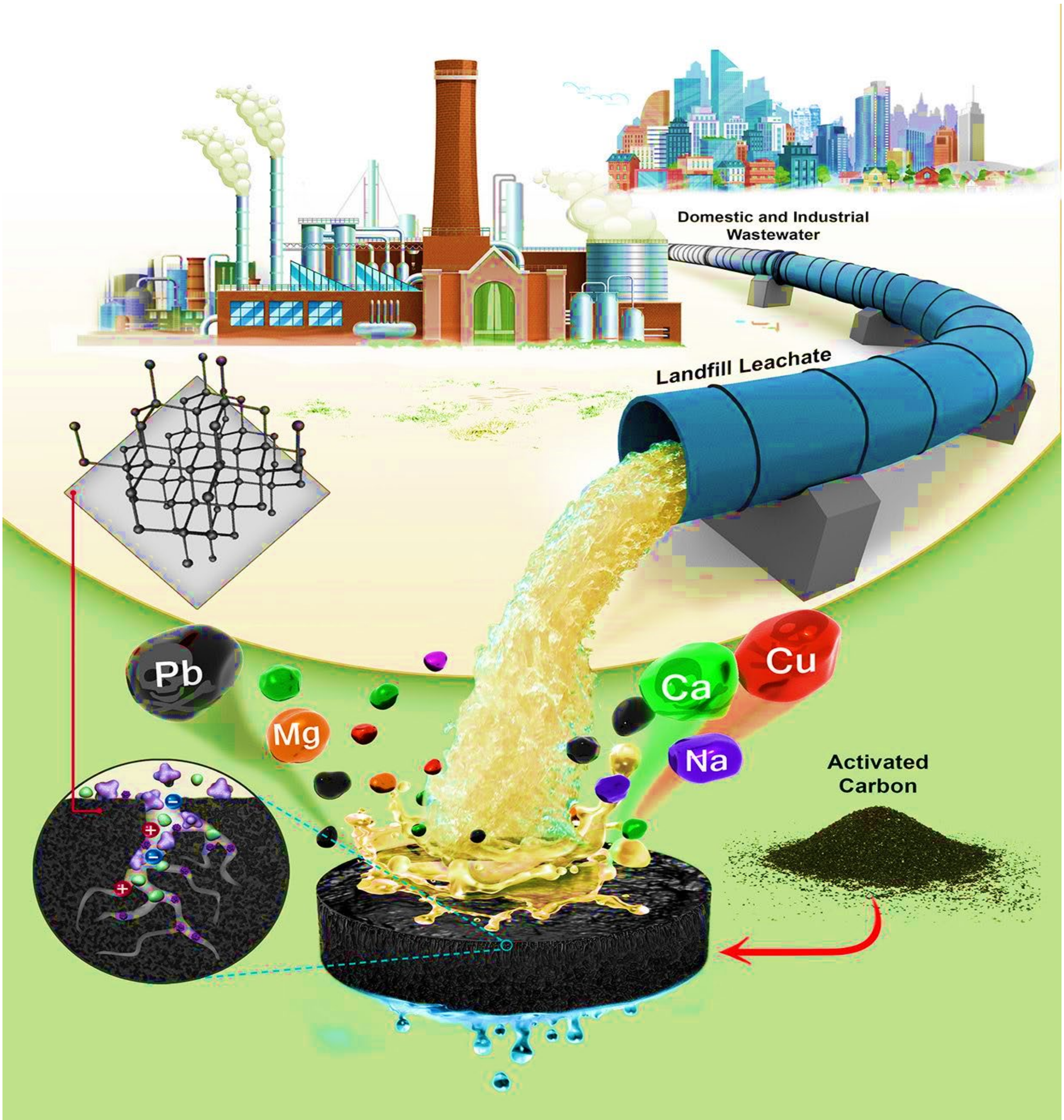

Graphical Abstract

Abstract

The challenge of effectively managing the discharge of metal ions into aquatic environments, which poses a significant risk to both human health and ecosystems, persists despite the availability of various analytical tools and techniques. There are limitations of existing separation technologies and the inefficacy of hydrogel materials in removing low molecular weight contaminants, such as metal ions, in aqueous solutions. This study added carbon powder to the hydrogel membrane to reduce the low-mechanical strength and drying problems and increase its capacity for adsorbing ionic and non-ionic substances. The study introduced a novel carbon-based aluminium hydroxide hydrogel for wastewater filtration. CG was characterized using various analytical techniques, including examining surface morphology, elemental analysis, surface functional groups, and surface charge. These analytical tools provided a comprehensive understanding of the properties and performance of the CG. The effects of different carbon-based hydrogel (CG) concentrations on water flux and ion rejection were evaluated in a gravity filtration setup. Experiments investigated the influence of different ion concentrations, activated carbon (AC) concentration, centrifugation, water flux, and rejection on removing heavy metals from synthetic and natural wastewater. The pure water flux of the hydrogel membrane was 120 LMH. The results indicated that an AC concentration of 4 g/L in the aqueous solution is optimal for heavy metals removal, with 99.9% removal for Pb^{2+} and Cu^{2+}, 84% rejection for Ca^{2+}, and 85% rejection for Mg^{2+} in 10 mg/L of synthetic water. Besides, the 4 g/L AC hydrogel membrane removed 90% of Ni, Zn, Pb, As, and Cu ions and 53% of the total organic carbon from leachate wastewater.

Keywords: Carbon-based hydrogel, Landfill leachate, Separation removal, Wastewater, Filtration

1. Introduction

Heavy metals, insecticides, pharmaceutical residues, herbicides, and other chemical compounds are common environmental pollutants. Heavy metals are released into the environment from numerous sources, including cosmetics, roofing materials, automobile brake pads, water pipelines, and industrial effluent discharge [1]. These contaminants pose a serious threat to aquatic ecosystems and human health, and it is crucial to develop effective measures to reduce their presence in the environment [2].

Different technologies have been proposed for treating heavy metal ions in water, with varying levels of efficiency and cost. Some techniques utilized to purify contaminated water include electrochemical treatment, filtration using membranes, the combination of coagulation and flocculation, chemical precipitation, ion exchange, flotation, and adsorption [3, 4]. Membrane technologies are renowned for the high rejection efficiency of metal ions from solution. Still, their significant drawbacks are high capital and operation costs, generating secondary brine wastewater, and requiring hands-on experience [5]. Despite the simplicity of implementation and low cost, using adsorbents for heavy metal rejection is considered one of the most effective physicochemical methods due to its regenerative nature [6]. The adsorbents zeolites, biochar, carbon nanotubes, cellulose nanofibers, granular/powdered AC, and modified AC have been studied to treat heavy metals. Using AC as an adsorbent in wastewater treatment is appealing due to its high pore volume and large surface area. Despite its potential, adsorption technologies have limitations in their ability to remove heavy metals from wastewater effectively, and the regeneration process for reuse can result in secondary contamination [7].

The hydrogel technology was recently suggested for metal ions rejection from aqueous solutions, particularly biobased hydrogels have recently attracted attention [8-10]. A wealth of literature on the hydrogel treatment technique for ion rejection exists. For instance, Sharokhi-Shahkari et al. conducted a study to assess the efficacy of commercial activated carbon (CAC) and tire-derived activated carbon (TAC) to remove Pb^{2+}, Cu^{2+}, and Zn^{2+} from synthetic water. The findings revealed that tire-derived activated carbon (TAC) exhibited a superior ability to remove heavy metals $Cu^{2+,}$ Zn^{2+}, and Pb^{2+} from synthetic water compared to commercial activated carbon (CAC). The monolayer adsorption capacities of TAC were shown to be 185.2 mg/g, 322.5 mg/g, and 71.9 mg/g for Cu^{2+}, Pb^{2+}, and Zn^{2+}, respectively, which were notably higher than those of CAC, which were recorded as 42.5 mg/g, 15.0 mg/g, and 14.0 mg/g for Pb^{2+}, Cu^{2+}, and Zn^{2+}, respectively [7]. Mu and co-workers focused on removing heavy metals by courier in AC hydrogel. The results show that the maximum adsorption capacity for Cu^{2+}, Mn^{2+}, Pb^{2+}, and Cd^{2+} was 161 mg/g, 75, 72, and 41 mg/g at 1000 mg/L metals concentration [11]. Perumal and co-workers comprehensively overview the possible release of multi-heavy metal ions (Hg^{2+}, Pb^{2+}, Cd^{2+}, and Cr^{3+}) from the spherical chitosan-gelatin hydrogel. The rejection was 84.7% for Hg $^{2+}$, 8.7% for Pb $^{2+}$, 0 % for Cd^{2+}, and 6.7% for Cr^{3+} at the initial concentrations 3.60, 3.68, 4.38, and 3.7 mmol [12]. S. Queiroz et al. investigated the synthetic AC from acai seed as a raw material. The results show that the modified AC outperformed conventional AC with a higher rejection of 86% for Pb^{2+},69% for Fe^{2+}, and 8% for Mg^{2+} due to their rich surface chemistry [13]. Despite the wide range of developed technologies for metal ions rejection from solution, most of these technologies suffer from high operating costs, generating a secondary waste stream or poor rejection rate [14-16]. In contrast, conventional hydrogels showed a limited rejection rate of metal ions from aqueous solutions. While numerous publications exist on hydrogels, hydrogel membranes in biomedicals, and hydrogels for water and wastewater treatment, comparatively fewer publications exist on using hydrogel membranes for water and wastewater treatment [17]. Hydrogel membranes have shown great potential for various water and wastewater treatment applications, including oil/water separation [18], membrane filtration/desalination [19-21], adsorption [20], and catalysis [22]. Previous studies have investigated the adsorption capabilities of hydrogel membranes in aqueous solutions [23]. In contrast, others have critically reviewed using (innovative) polymeric materials for controllable oil/water separations, highlighting the benefits of hydrogel membranes [24]. Hydrogel membranes can be prepared using different methods, resulting in varying levels of super hydrophilicity/lipophilicity [25]. In oil/water separation, these membranes have demonstrated high flux and rejection performance. Their excellent antifouling properties make them suitable for filtration and desalination [26]. The porous structure of hydrogels provides a large comparative area, allowing for interfacial evaporation. Furthermore, hydrogel membranes have been explored for their catalytic performance [27]. These findings highlight the versatility and potential of hydrogel membranes in various water and wastewater treatment applications [17]. In a study by Lu et al. [28], a hydrogel membrane exhibited catalytic and filtration properties. The catalytic hydrogel membrane demonstrated a separation efficiency of 90% and a catalytic efficiency of 99%. Furthermore, incorporating a hydrogel layer into membranes resulted in the exceptional rejection of aqueous pollutants and high permeability [28]. Hu et al. [29] produced a polyelectrolyte complex hydrogel membrane by self-assembling two polysaccharides, salecan and carboxymethyl chitosan, with opposite charges. The resulting membrane exhibited an adsorption capacity of 418.4 mg/g for Pb^{2+} and retained 95% of its capacity after 5 cycles. Graphene oxide/alginate hydrogel membranes were also used as adsorbents and showed a maximum adsorption capacity of 327.9 mg/g for Pb^{2+} and 118.6 mg/g for Cr^{3+} [29]. A hybrid hydrogel nanocomposite membrane was created by Baruah et al. [30] by conjugating chitosan with oxidized carbon dots synthesized from 11-mercaptoundecanoic acid. Through adsorption, the membrane could remove 68.01% of Ca^{2+} and 56.35% of Mg^{2+} from pond water. In a separate study, a PVA hydrogel membrane demonstrated an adsorption capacity of 45.8 mg/g for Sr^{2+} and successfully removed 87% of it during the filtration of synthesized radioactive wastewater containing 5 mg/L Sr^{2+} and 250 mg/L Ca^{2+} [30].

Unique characteristics of AC, such as large surface area, appropriate pore size distribution, a wide variety of surface functional groups, and relatively high mechanical strength, contribute to its excellent adsorption [31]. Therefore, as a cross-linker, AC powder could improve the hydrogel filter's physicochemical properties and permselectivity.

For the first time, the current study investigated the feasibility of carbon-based aluminium hydroxide hydrogel (CG) for water and wastewater treatment. Aluminium hydroxide polyhydrate hydrogel was prepared as the base material for water filtration. Then, AC was added to enhance the physicochemical characteristics of the hydrogel filter, such as mechanical strength, drying and cracking problems, and rejection of metal ions. Synthetic and landfill leachate wastewater solutions were tested for the CG membrane treatment from metal ions and organic matter. Furthermore, the study evaluated the impact of AC loading on the water flux and rejection of the hydrogel membrane and the membrane performance in multiple filtration cycles. The current study suggests a gravity-driven carbon-based aluminium hydroxide hydrogel membrane to reduce the operation cost for wastewater filtration. The gravity-driven hydrogel membrane does not require high-pressure pumps or expensive infrastructure to operate. Besides, the hydrogel membrane operates in a dead-end mode, eliminating brine wastewater generation. The hydrogel exhibited a steady performance in the consecutive filtration cycles, with 99% copper rejection in four cycles.

2. Materials and method

2.1 Materials

The analytical-grade materials utilized in the study were obtained from suppliers without any alterations. AC powder with an average molecular weight of 12.01 g/mol and a particle size of 100 mesh was procured from Sigma-Aldrich (Australia) to prepare CG. Aluminium sulfate (342.15 g/mol), sodium bicarbonate (84.01 g/mol), sodium chloride (NaCl), magnesium chloride ($MgSO_4$), copper sulfate ($CuSO_4$), lead nitrate ($PbNO_3$), and calcium chloride ($CaCl_2$) were used in preparing and testing the CG hydrogel membrane were supplied by Chem-supply, Australia. Deionized water (Milli-Q® Merck) was utilized throughout the experiments to prepare diluted NaCl, $MgSO_4$, $CuSO_4$, $CaCl_2$, $PbNO_3$, and CG. All chemicals were used in their original form as received from the suppliers. The materials used are analytical grade and used as suppliers provide without modifications. Biologically treated landfill leachate wastewater from the Hurstville Golf Centre in Sydney, Australia, was used in testing the rejection of the CG hydrogel membrane **(Table 1**). The landfill wastewater was stored in a refrigerator.

Table 1 The main characteristic of landfill leachate collected from Hurstville Golf Centre

Parameter	Value	Unit
Turbidity	34	NTU
Colour	Light brown	
pH	7.82	
Conductivity	12.10	mS/cm
Total dissolved solids (TDS)	5550	mg/L
Total organic carbon (TOC)	149.2 ±5	mg/L
Total carbon (TC)	204 ±5	mg/L
Chemical Oxidation Demand (COD)	150	mg/L
Total iron	≤5	mg/L
Salinity	1.75± 0.1	g/L

Na	1600	mg/L
K	99.73	mg/L
Mg	81.69	mg/L
Ba	1	mg/L
Ca	179.71	mg/L
Mn	0.1	mg/L
Ni	3.27	mg/L
Zn	4.4	mg/L
Pb	6.63	mg/L
As	5.69	mg/L
Cu	6.27	mg/L

2.2 GC hydrogel membrane preparation

Aluminium hydroxide polyhydrate hydrogel (AHG) was prepared from the reaction of aluminium sulfate and sodium bicarbonate according to the following equation:

$Al_2(SO_4)_3 + Na_2CO_3 + H_2O \rightarrow Al\ (OH)_3 + Na_2SO_4 + CO_2$ [1]

A step-by-step diagram of the hydrogel membrane fabrication is presented in Figure 1. Initially, 36.4 g of aluminium sulfate was dissolved in deionized (DI) water. A beaker of a suitable size was chosen to accommodate the solution, and DI water was added to it. The aluminium sulfate was then gradually added to the water while stirring continuously using a magnetic stirrer (Labco Digital 20L). The stirring was performed for one hour to ensure complete dissolution and uniform mixing of the aluminium sulfate in the solution. Separately, 53.76 g of sodium bicarbonate was dissolved in DI water at a temperature of 30°C. A beaker of a suitable size was used, and DI water was added to it. The sodium bicarbonate was gradually added to the water while stirring, and the stirring process was continued for 30 minutes to ensure complete dissolution. After the individual solutions were prepared, the sodium bicarbonate solution was added gradually to the aluminium sulfate solution. This step was carried out in a separate beaker with a one-litre capacity. The gradual addition of sodium bicarbonate solution helps form the aluminium hydroxide polyhydrate hydrogel. Stirring was continued during the addition to ensure proper mixing of the solutions. Once the sodium bicarbonate solution was added to the aluminium sulfate solution, the resulting solution was left undisturbed for two to three weeks. During this time, polymerization of the hydrogel occurred, forming the aluminium hydroxide polyhydrate hydrogel. This step allowed the hydrogel to mature and stabilize. In the final step, carbon-based hydrogel membranes were prepared using activated carbon (AC). For each membrane, 1 g, 2 g, 3 g, and 4 g of AC were added separately to 1000 ml of DI water. The mixture was then sonicated for six hours using a digital ultrasonic bath (Thermo Scientific). This step aimed to enhance the properties and performance of the hydrogel membranes by incorporating AC. Throughout the hydrogel synthesis process, ambient conditions of 52% humidity and 22 °C were maintained to ensure consistency in the preparation of the hydrogel membranes. The prepared hydrogel membranes with AC concentrations of 1 g/L, 2 g/L, 3 g/L, and 4 g/L were denoted as 1CG, 2CG, 3CG, and 4CG, respectively.

A schematic diagram of the experimental hydrogel filtration apparatus is shown in **Figure 1**. The filtration experiments were conducted in a 15 cm length × 6.5 cm diameter cylinder of HDPE material to facilitate visual observation. The head of the feed solution controls water flux in the gravity-driven CG hydrogel. Filtration experiments were conducted at room temperature, 22 ^{o}C ± 3 ^{o}C. Unlike polyamide membranes, a moderate feed temperature increase insignificantly affects the inorganic CG hydrogel membrane. The hydrogel was set on a 35-mesh fabric cloth supported by a perforated screwed cap placed at the bottom of the filtration cylinder to hold the hydrogel membrane. To investigate the effect of the centrifugation of CG, 50 ml of CG was centrifuged at 2000 to 9000 rpm speeds with 1000 rpm speed intervals, while the supernatant was analyzed and discarded at the end of the centrifugation cycle. The rejection percentage (%R) of different ions such as Pb2+, Mg2+, Cu2+, and Ca2+ions were calculated following Equation 1 below:

$$\%R= (c_i-c_e)/c_i \quad *100 \qquad (1)$$

In Equation 1, Ci is the initial concentration (mg/L), and Ce is the concentration at the final equilibrium (mg/L).

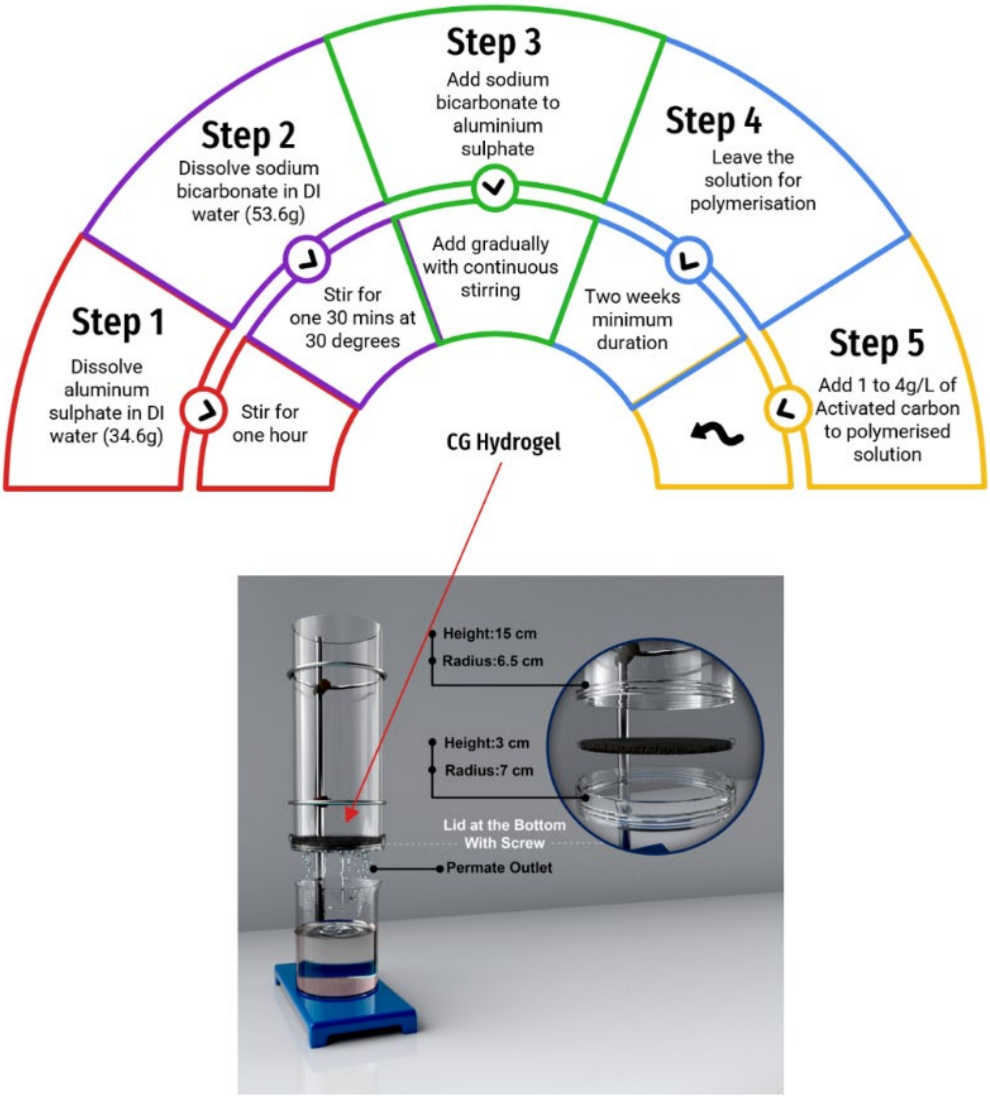

Figure 1: Schematic diagram of the filtration apparatus and setup of the 15 cm × 6.5 cm cylinder for CG experiments

2.3 Analytical methods

The Thermo Scientific Nicolet (ThermoScientific, Sydney, Austalia) 6700 FT-IR (Fourier Transform infrared spectroscopy) spectrometer was utilized to investigate the characterization of carbon-based filtration through FT-IR analysis in the 400-4000 cm^{-1}. The sample of CG was dried before testing, and each scan was produced from an average of 30 scans. The morphology of the CG hydrogel membrane was examined using Field emission scanning electron microscopy (FE-SEM) from Zeiss Elvo (Zeiss Evo LS15). The synthetic water was analyzed using ICP-MS (inductively coupled plasma spectroscopy) from Agilent Technologies. The zeta potential of the CG hydrogels was calculated using the Nano-ZS Zeta-sizer from Malvern Analytical. The surface area of the samples was determined through the BET (Brunauer-Emmett-Teller) method of nitrogen adsorption-desorption isotherms. The CG solutions were centrifuged using a Sigma centrifuge (model 2-16KL) for hydrogel dewatering and compaction.

2.4 Characterization of CG Hydrogel

CG hydrogel was characterized for physical and chemical properties to understand the mechanisms of divalent and monovalent metal ions rejection from solutions to evaluate their physical and chemical properties. The BET (Brunauer-Emmett-Teller) results showed that 4CG poses a significant specific surface area of 756.92 m^2/g, almost 30 times larger than the specific surface area of AHG 25.73 m^2/g. Furthermore, BET analysis revealed that the pore volume of 4 CG is 1.66 cc/g. Sample HG has the lowest pore volume (0.076 cc/g) and surface area (25.731 m2/g) (Table S1, supplementary information). Consequently, its capacity for ion removal may be limited compared to the other samples. Increasing the concentration of activated carbon on HGs can directly impact the pore volume and surface area, thus influencing its adsorption capabilities. When the concentration of activated carbon is increased, the available pore volume also tends to increase (0.195 cc/g to 1.64 cc/g). Higher concentrations result in more activated carbon particles, providing more space for adsorption. Consequently, the increased pore volume allows a larger number of molecules or ions to be adsorbed onto the surface of the activated carbon. Besides, the surface area of activated carbon is closely linked to its adsorption capacity. As the concentration of activated carbon increases, the overall surface area also tends to increase from 106.536 m^2/g to 756.919 m^2/g for 1CG to 4CG. Higher concentrations lead to more activated carbon particles, resulting in a greater total surface area for adsorption. The increased surface area provides more active sites for the interaction and adsorption of molecules or ions, enhancing the adsorption capacity of the activated carbon material.

FTIR spectra analysis was conducted on the CG to gain further insight into the rejection mechanisms. The results of the Fourier Transform Infrared Spectroscopy (FTIR) analysis for the HGs (aluminium hydroxide hydrogel) filter and CG (Carbon- aluminium hydroxide hydrogel membrane) provide insights into their chemical compositions and potential interactions with metal ions. For the HGs, the FTIR analysis revealed peaks at 510 cm^{-1} and 1082 cm^{-1}, consistent with $Al(OH)_3$. These peaks indicate the existence of Al-O bonds within the HGs. A prominent peak at 3465.27 cm-1 also suggests the stretching vibrations of surface and interlayer water molecules and hydroxyl groups (Fig 2a). In the case of the CG, the FTIR analysis exhibited several characteristic features. An absorption band around 3255 cm^{-1} was observed, which can be attributed to the stretching vibration of hydroxyl groups from water, suggesting the presence of water molecules and hydroxyl groups on the CG surface. The FTIR spectrum also displayed peaks at 941 cm^{-1} and 678 cm^{-1}, corresponding to the aromatic C-H bending vibration and Al single bond stretching vibrations, respectively. These peaks indicate the presence of aromatic compounds and aluminium bonds within the CG. Moreover, the absorption peak at 1556 cm^{-1} suggests the existence of aromatic C=C groups, while the absorption peak at 1118.7 cm^{-1} indicates the presence of C-O-H functional groups. Overall, the FTIR analysis provides valuable information about the chemical characterization of the HGs and CG. The observed peaks and bands indicate the presence of specific chemical bonds, such as Al-O bonds in the HGs and aromatic compounds in the CG. These findings suggest potential mechanisms for the adsorption of metal ions through the interaction of these functional groups on the filter surfaces. In contrast, the presence of group C-O-H was suggested by an absorption peak at 1118.7 cm^{-1} (Fig 2b)

The X-ray Diffraction (XRD) analysis is primarily utilized to uncover information regarding the phase and crystal structure of materials. The outcome of the XRD pattern for 1CG to 4CG concentrations is demonstrated in **Figure 2c**, revealing that all CG hydrogel samples were found to possess an amorphous-microcrystalline nature. The X-ray Diffraction (XRD) analysis is a widely used technique for studying the crystal structure and phase identification of materials. In the case of the hydrogel membrane sample (1CG to 4CG), Figure 2c displays the XRD pattern obtained from the analysis. Amorphous materials lack a well-defined, periodic arrangement of atoms, resulting in a diffraction pattern of broad peaks.

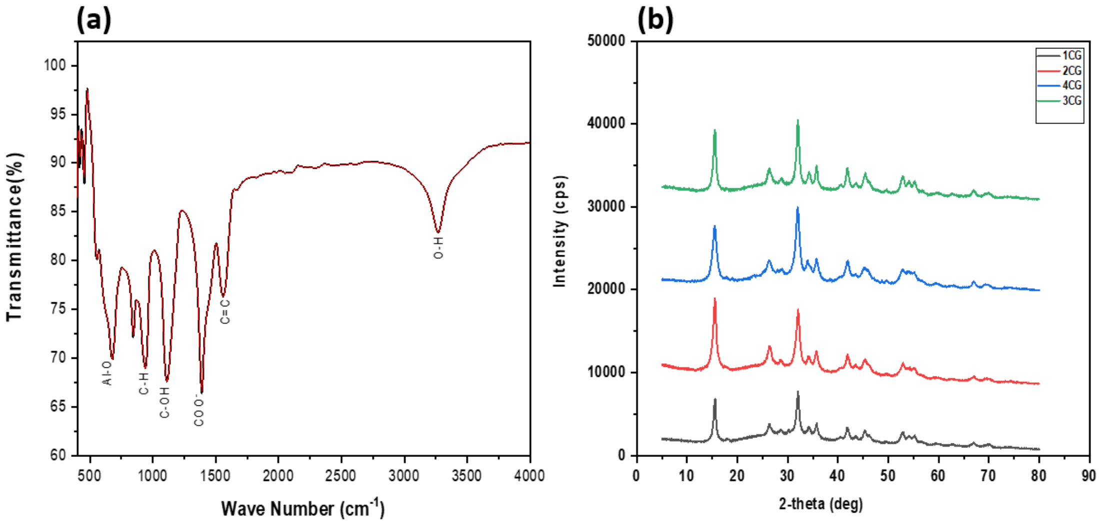

Figure 2: (a) FTIR Fourier-transform infrared spectroscopy (FTIR) spectrum of 4g/L CG (b) XRD spectra of 1 CG, 2 CG, 3 CG, and 4 CG in the room temperature

The XRD pattern for the CG hydrogel membrane samples reveals specific peaks at certain 2θ angles. These peaks indicate the presence of crystalline phases within the amorphous-microcrystalline structure. In particular, the XRD patterns show two prominent peaks at approximately 2θ angles of 15.29 and 37 degrees, corresponding to the crystallographic planes of aluminium hydroxide. The presence of these peaks suggests that the aluminium hydroxide within the hydrogel samples possesses a crystalline structure. The position and intensity of the peaks in the XRD pattern provide information about the spacing between crystal planes and the relative abundance of different crystallographic phases. Furthermore, it is worth noting that the XRD pattern for the CG hydrogel samples also exhibits peaks at 2θ angles of 15.29 and 36.84 degrees. These additional peaks may indicate the presence of other crystalline phases or the formation of microcrystalline structures within the amorphous matrix of the hydrogel. Overall, the XRD analysis confirms that the CG hydrogel samples possess an amorphous-microcrystalline nature, with both amorphous and crystalline phases. The specific peaks observed in the XRD patterns provide insights into the crystal structure and phase composition of the hydrogel samples, contributing to a better understanding of their properties and behaviour.

This shift in peak angle was attributed to the AC coating on the surface of aluminium hydroxide. The peaks observed at 26 degrees were from the AC. Near 15 degrees were caused by the adsorbents' micro-porous and micro-crystalline nature, resulting from the multi-layer stacking of micro-crystalline structures resembling AC. Overall, the relative intensities of the peaks were almost similar for 2CG, 3CG and 4CG, and slightly higher intensities were observed for these peaks compared to 1CG. The results of the Fourier Transform Infrared Spectroscopy (FTIR) analysis for the HGs (aluminium hydroxide hydrogel) filter and CG (Carbon -aluminium hydroxide hydrogel membrane) filter provide insights into their chemical compositions and potential interactions with metal ions **(Figure S.1 Supplementary information**). For the HGs filter, the FTIR analysis revealed peaks at 510 cm-1 and 1082 cm-1, consistent with Al (OH)3. These peaks indicate the existence of Al-O bonds within the filter material. Additionally, a prominent peak at 3465.27 cm-1 suggests the stretching vibrations of surface and interlayer water molecules as well as hydroxyl groups. This peak indicates the presence of these functional groups on the HGs surface, which could play a role in attracting metal ions. In the case of the CG, the FTIR analysis exhibited several characteristic features. An absorption band around 3255 cm-1 was observed, attributed to the stretching vibration of hydroxyl groups from water, indicating the presence of water molecules and hydroxyl groups on the CG filter surface. The FTIR spectrum also displayed peaks at 941 cm-1 and 678 cm-1, corresponding to the aromatic C-H bending vibration and Al single bond stretching vibrations, respectively. These peaks indicate the presence of aromatic compounds and aluminium bonds within the CG.

Moreover, the absorption peak at 1556 cm-1 suggests the existence of aromatic C=C groups, while the absorption peak at 1118.7 cm-1 indicates the presence of C-O-H functional groups. Overall, the FTIR analysis provides valuable information about the chemical characterization of the HGs and CG filters. The observed peaks and bands indicate the presence of specific chemical bonds, such as Al-O bonds in the HGs filter and aromatic compounds in the CG. These findings suggest potential mechanisms for the adsorption of metal ions through the interaction of these functional groups on the filter surfaces.

Energy-dispersive X-ray spectroscopy (EDS) and scanning electron microscopy (SEM) were taken to detect the CGs elemental composition by Zeiss Evo-SEM with an acceleration voltage of 15 kV for EDS collection. SEM examined the surface characteristics of CG membranes coupled with EDS (**Figure 3**). The SEM micrographs of CG membranes showed that the morphology changed with increasing concentrations of AC. At low concentrations, the carbon particles appear to have dispersed evenly on the hydrogel surface (Figure 3a), maintaining its overall integrity. However, at higher concentrations, a large amount of activated carbon can lead to agglomeration or clustering of particles, as evident in Figures 4b, 4c and 4d. The 4CG surface structures become more compact, smoother, and less porous compared to the samples 1CG, probably, due to the increased number of AC on the surface, which altered its original structure. The particles appeared to be agglomerated due to clustering and higher adsorption capacity. Incorporating activated carbon particles into the hydrogel can also introduce surface irregularities (Figures 4b, 4c and 4d), increasing the roughness of the membrane's surface. This roughness can provide additional sites for the adsorption of different contaminants in the feed solution. At low concentrations, the carbon particles have dispersed evenly on the hydrogel surface (Figure 3a), maintaining its integrity. However, at higher concentrations, a large amount of activated carbon can lead to agglomeration or clustering of particles, as evident in Figures 4b, 4c and 4d.

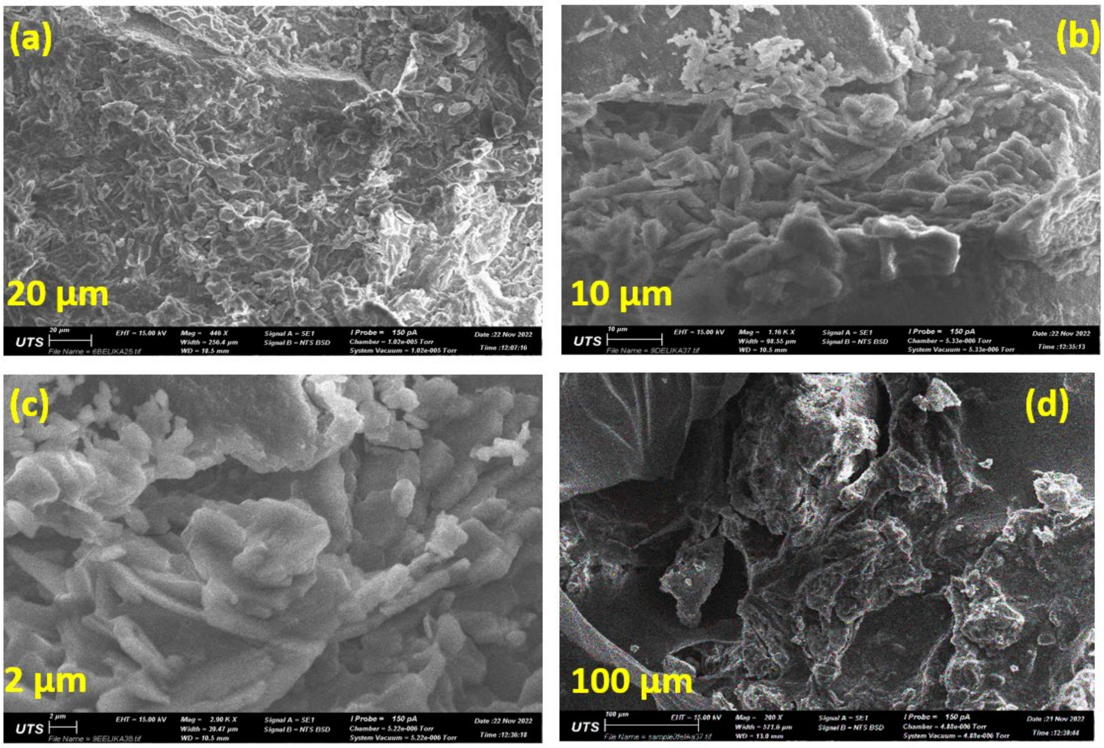

Figure: 3 SEM image of CG membranes at different concentrations of AC under 30000 magnitudes at room temperature (22 °C) (a) 1CG (b) 2CG (c) 3CG (4) 4CG

Energy dispersive X-ray spectroscopy (EDS) analysis was attained to determine the elemental composition of the CG. EDS analysis clearly shows the presence of C, O, and Al (**Figure S1a**, Supplementary information, S.1). EDS X-ray shows a small peak of sodium ions, which can be assigned to the sodium bicarbonate used during the CG preparation. As the concentration of AC increases, so does the percentage of carbon in the hydrogel membranes **(Figure S1b to S1d, Supplementary information S.1).** The mass percentage of each element within/on CGs is explained in **Table 2**. In **Figure S1e (Supplementary information S.1)**, it is noticeable that there are substantial peaks located at 0.5 kV (Kα, Ca) and 3.5 kV (Kβ, Ca), indicating the adsorption of calcium ions. These peaks signify the energy levels of the calcium ions as they are absorbed onto the surface of the AC. Similarly, in **Figure S1 f-h (Supplementary**

information S.1), prominent peaks can be seen at 0.5 kV (Kα, Cu) and 8 kV (Kβ, Cu), 1 (Kβ, Mg) for Cu^{2+} and Mg^{2+} ions, which represent adsorption for Cu^{2+} and Mg^{2+} ion adsorption, respectively. Also, it can be seen in **Figure S1.H (Supplementary information S.1)** that prominent peaks occur at 2.5 kV (Kα, Pb) and 10.5 kV (Kα, Pb) for Pb^{2+} ions representing adsorption to CG. The carbon content was significantly increased in Fig. S1e, S1g, and significantly decreased in Fig. S1h. This can be attributed to the high affinity of Ca and Cu to carbon compared to Pb; calcium and copper have higher affinities for carbon than pb. In contrast, Ca has a higher affinity than Cu; therefore, the carbon content in FigS1e is higher than in Figure S1g.

Table 2 Composition of the element of CG and 4CG after treatment of 1000 mg/L Ca^{2+}, Mg^{2+}, Pb^{2+}, Cu^{2+} feed solution

Sample Name	Elemental Composition wt (%)								
	C	O	Na	S	Al	Ca	Mg	Pb	Cu
1CG before treatment	11.42	57.84	11.96	0.31	18.47	-	-	-	-
2CG before treatment	12.68	56.53	10.74	0.20	19.85	-	-	-	-
3CG before treatment	12.72	56.51	10.72	0.20	19.85	-	-	-	-
4CG before treatment	18.31	56.77	12.69	0.02	12.20	-	-	-	-
4CG after treatment Ca	22.67	54.71	8.98	0.02	11.22	2.41	-	-	-
4CG after treatment Mg	13.56	59.58	5.58	0.93	17.92	-	2.33	-	-
4CG after treatment Cu	20.23	59.97	6.57	1.23	11.91	-	-	-	6.13
4CG after treatment Pb	7.96	42.70	6.01	23.37	0.20	-	-	19.75	-

Electrostatic interactions between charged ions in the feed solution and the hydrogel membrane are critical for understanding the rejection mechanism. **Figure 4** shows the surface zeta potential measurements for CGs. As a result of the carboxylic (single bond COOH), hydroxyl (single bond OH) of AC, and hydroxide of aluminium, the fabricated CGs had a negative zeta potential. The surface zeta potential increased with the increasing AC powder concentration in the CG from − 20.41 mV to − 36.58 mV for 1CG and 4CG, showing a 1.5 times increase in zeta potential due to the higher AC concentration. This increase in negative zeta promotes metal ions rejection and adsorption on CG's surface.

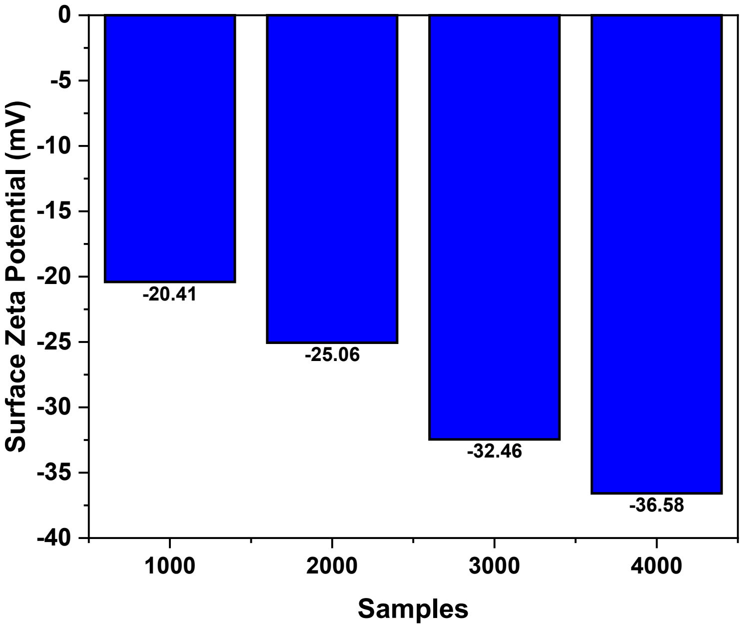

Figure 4: Surface zeta potential at different concentrations of AC in the CG from 1 to 4 CG

2.5 Mechanical strength of CG Hydrogel

According to previous research [32], hydrogel has poor mechanical strength and is prone to cracking when subjected to low hydraulic pressure. Hydrogel's mechanical fragility has a negative effect on filter cleaning and backwash. The hydrogel's performance also deteriorates when fractures appear on its surface because they create pathways for contaminants to bypass the filtration system. In this study, AC was considered to improve the mechanical strength of hydrogel and adsorption capacity. According to earlier research [33-35], carbon materials act as cross-linkers with a potent interaction with polymer chains. This property will lessen the challenges associated with hydrogel drying when AC is added to the hydrogel matrix. In addition, carbon additions improved the water-holding ability of polymer materials [36]. Using a rotating shear rheometer to test the material's mechanical strength revealed that hydrogel containing AC is more fracture-resistant. **Figure 5** depicts the rheology results of the different concentrations of AC hydrogel at room temperature.

The hydrogel's rheological properties strongly influence its membrane performance [37, 38]. The balance between viscosity and elasticity influences the ability of the hydrogel membrane to recover its original shape after deformation. A hydrogel membrane should have suitable viscoelasticity to maintain its structural integrity when subjected to mechanical stresses. The preliminary rheology results demonstrate that adding AC additives to the hydrogel increases its mechanical strength. AC is a porous material that can exhibit viscoelastic behaviour, combining viscous and elastic. The concentration of AC can influence its viscoelastic properties. At low concentrations, for example, AC suspensions exhibit more elastic behaviour, i.e. tend to return to the original shape after being subjected to deforming stress due to the weak interparticle interactions between the AC particles. At higher concentrations, the interparticle interactions become more robust, and the suspensions exhibit more viscous behaviour, meaning they tend to deform permanently under stress. The shear stress versus shear rate graph for an AC suspension at high concentration will show a non-linear relationship typical of non-Newtonian fluids (**Figure 5a**). For all tested samples, it was noted that as the shear rate increased, the viscosity decreased, and the shear stress increased **(Figure 5b).**

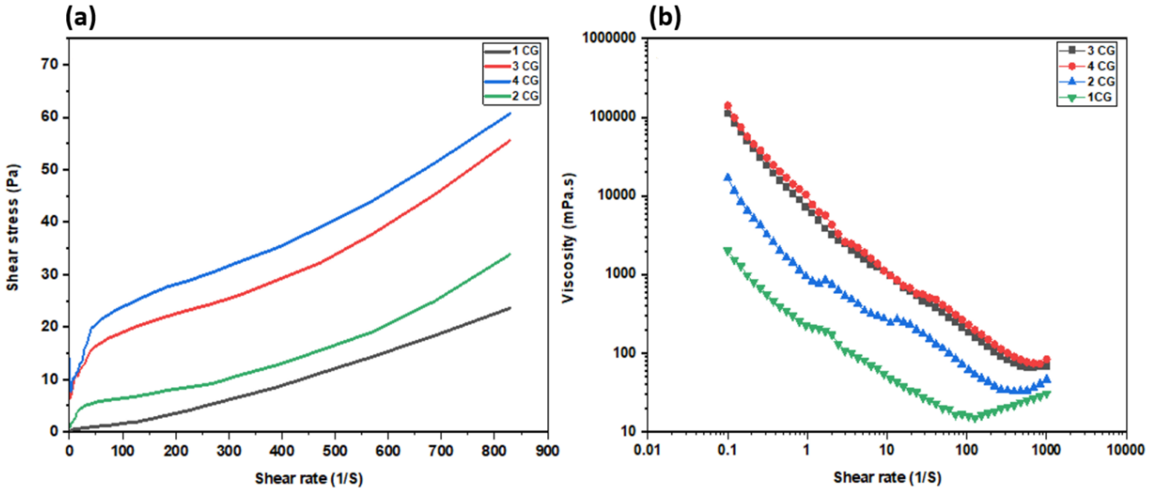

Figure 5: Mechanical strength of different concentrations of AC at room temperature (a) stress rate vs shear rate (b) viscosity vs shear rate

The shear stress-shear rate curve for the synthesized CG hydrogel membranes shows a rapid increase in apparent viscosity as the shear rate decreases, indicating shear-thinning behaviour. CG is a viscoelastic polymer, meaning it exhibits both viscous and elastic properties. When AC is dissolved in aluminium hydroxide polyhydrate hydrogel, the polymer chains form a network that contributes to the overall viscosity of the solution. As shear is applied, chains are rearranged, and the network is disrupted, leading to a decrease in viscosity and an increase in fluidity; this effect is known as shear thinning. The degree of shear thinning depends on the concentration of AC in aluminium poly hydrate hydrogel and the magnitude of the applied shear. Higher concentrations of AC result in a more pronounced network structure, which means the degree of shear thinning is higher.

3. Results and discussion

3.1. Water flux of CG Hydrogel membrane

Several factors impact the hydrogel water flux, such as feed concentration, hydrogel compaction, feed temperature, solute size and shape, viscosity, and ionic interactions. Before the filtration tests, the CG solution was prepared and cast on a fabric support layer (35 mesh) with and without hydrogel centrifugation. DI water and synthetic feed solution with various divalent ions were tested for the hydrogel membrane filtration process to investigate the impact of feed composition on the water flux. The CG membrane thickness was about 1mm, and each test was repeated twice to confirm the results.

Initially, the water flux of CGs was tested at 0.01 bar (circa 10 cm head) using a DI water feed solution. **Figure 6a** shows the effect of centrifugation at 2000 to 9000 rpm, with a 1000 rpm interval, on the performance of the CG filter containing 1 to 4 g/L AC (1CG to 4CG hydrogel membranes) with DI water feed solution. Results show a decrease in water flux by increasing the centrifugation speed from 0 rpm to 9000 rpm or increasing the concentration of AC in the CG. For hydrogel tests without centrifugation, the water flux decreased from 312 LMH in the 1CG hydrogel membrane to 147.4 LMH in the 4CG hydrogel membrane. However, as the centrifugation speed was increased to 9000 rpm, the water flux decreased to 49.12 LMH for 1CG. This reduction in water flux could be attributed to the compaction of the hydrogel at higher centrifugation speeds. The pore analysis test showed that the hydrogel membrane pore volumes decreased from 1.66 cc/g to 0.268 cc/g due to the AC concentration increase from 1 g/L to 4 g/L. Likewise, the GC hydrogel membranes' porosity decreases with increasing the concentration of AC, resulting in more compacted CG media and hence a lower water flux. As shown in **Figure 6a**, increased AC concentration in the CG and increased centrifugation speed decreased the hydrogel membrane water flux. Specifically, there was more than a 60% reduction in water flux after centrifugation at 9000 rpm. A similar water flux decrease was observed in the CGs with 2, 3, and 4 g/L AC concentrations (**Figure 6**).

Experimental results with 10 mg/L of Pb^{2+} (**Figure 6b**) feed solution revealed that the water flux of CG membrane without centrifugation was 122 LMH for 1CG, 108 LMH for 2CG, 93 LMH for 3 CG, and 75 LMH for 4CG hydrogel membrane. In effect, the water flux in the 1CG was 1.5 times that in the 4CG. Similar results for lower water flux with increasing AC concentrations were achieved for Cu^{2+}, Mg^{2+}, and Ca^{2+} feed solutions, as presented in **Figures 6c, 6d, and 6e**. The lower water flux achieved in the CG containing higher AC concentration could be attributed to the decrease in CG's pore size at increased AC concentration, causing a sharp drop in water flux. There is a trade-off between CG's water flux and rejection (selectivity) due to the variation in centrifugation speeds and AC concentration in the CG hydrogel membrane.

On the other hand, there is an increase in the ions rejection rate when the CG hydrogel membrane contains high AC concentration and is processed at high centrifugation speeds due to the reduction in the pore size and CG compaction. Charged molecules and large particles could be held on the hydrogel surface due to electrostatic and physical hindrances. At the same time, small and low-charged ions enter the hydrogel pores and are separated by surface interactions (electrostatic and friction).

Figure 6f shows the water flux of DI, landfill leachate, and UA-60 NF membrane (Microdyn, Germany). The water flow rate dropped from 120 LMH for deionized water to 81.12 LMH and 72.40 LMH for GW and landfill leachate, respectively. Pore compression or hydrogel collapse can reduce adequate pore size and decrease water passage. The results show that the 4CG hydrogel membrane has a higher flux (72.40 LMH) than the current membrane UA-60 (50 LMH) at 5 bar pressure (**Figure 6f**) [39]. The problem of film contamination could be solved by soaking the hydrogel in a DI water solution to remove loose contaminants on the hydrogel surface. Chemical cleaning, although effective, it has disadvantages as it will generate additional waste streams and make the process energy intensive. Knowing that the hydrogel material is inexpensive (>$1 per m^2), chemical cleaning will increase the filtration cost and generate wastewater.

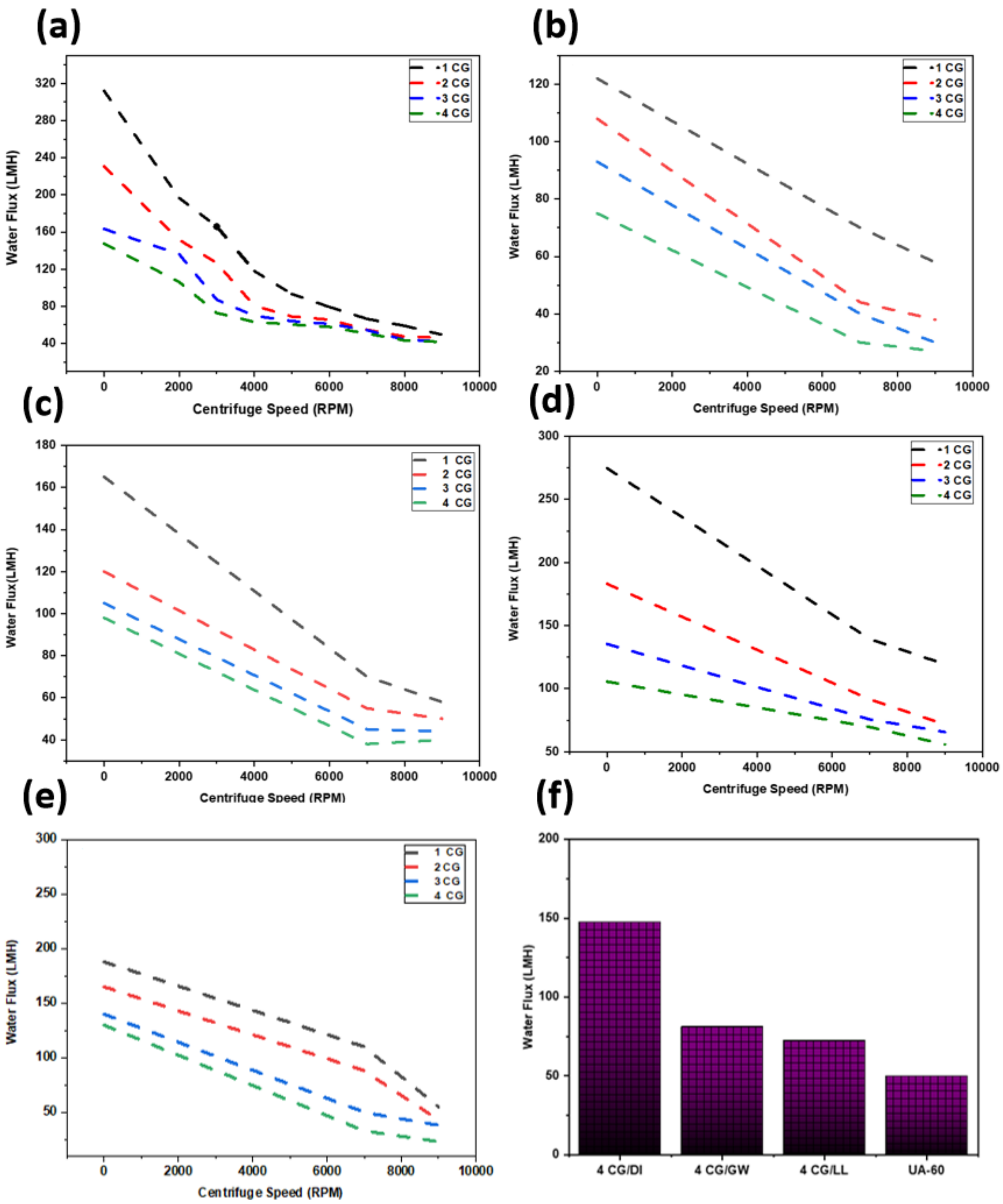

Figure 6: Water flux of metal ions at different concentrations of AC (a) DI water (b) 10 mg/L of Pb (c) 10 mg/L of Cu (d) 10 mg/L of Mg (e) 10 mg/L of Ca (f) 4CG for groundwater landfill leachate (LL) and UA-60 membrane for landfill leachate in the room temperature.

3.2 Synthetic feed treatment

This section investigated the rejection percentage of the CG hydrogel membrane to divalent ions from an aqueous solution. 10 and 1000 mg/L of Pb^{2+}, Mg^{2+}, Cu^{2+}, and Ca^{2+} were dissolved in DI water and filtered through the CG hydrogel membrane of 1 to 4 g/L AC. The impact of centrifugation on the rejection rate of divalent ions by the CG filter was investigated using a 15 cm high filtration column of 0.4L capacity.

Inductively Coupled Plasma measured the final concentrations of Pb^{2+}, Mg^{2+}, Cu^{2+}, and Ca^{2+} in the product water. The results are illustrated in (**Figures 7a-7d**) for 10 mg/L of metal ions and **(Figure 7e-7h)** for 1000 mg/L of metal ions.

Figure 7 shows that the permeate concentration decreased as the AC concentration in the hydrogel increased or when the CG hydrogel membrane was prepared at elevated centrifugation speeds**.** The 4CG hydrogel membrane achieved the highest ion rejection from the feed solution. The 4CG hydrogel membrane, without centrifugation, achieved rejection efficiencies of 99.9%, 99.9%, 84%, and 90%, respectively, for Pb^{2+}, Cu^{2+}, Ca^{2+}, and Mg^{2+} (**Figure 7a-7d**). For the 10 mg/L feed solution, CG hydrogel membranes with and without hydrogel centrifugation showed high rejection efficiencies for Pb^{2+} and Cu^{2+} (**Figure 7a-7b**). For example, at 9000 rpm, the rejection efficiency of Pb^{2+} and Cu^{2+} for CG hydrogel membranes was over 99.9%. The 1CG hydrogel rejection of Cu^{2+} ions increased from 98.7% without centrifugation to 99.5% at 9000 rpm centrifugation speed. Similarly, for Ca^{2+} and Mg^{2+}, the rejection increased as the centrifugal force increased. At 9000 rpm, the 4CG hydrogel membrane rejection of Ca^{2+} was 94% and 98% for $Mg^{2+.}$

For 1000 mg/L feed solutions, it was observed that the rejection of Pb^{2+} and Cu^{2+} increased as the centrifugal force increased (**Figures 7e and 7f**). For all CG hydrogel membranes prepared at 9000 rpm, the rejection of Pb^{2+} was more than 93%, and 4CG hydrogel achieved the highest rejection of 97.4% (**Figure 7e**). The rejection of Cu^{2+} was over 95% for all CG hydrogel membranes at 9000 rpm, with 4CG hydrogel membrane achieving the highest rejection of 98.5% (**Figure 7f**). On the contrary, the removal efficiencies of Ca^{2+} and Mg^{2+} did not significantly improve as the centrifugal force increased (**Figure 7g and 7h**). For $Ca^{2+,}$ the highest rejection was observed with 4CG at 9000 rpm, with a value of 53.5%. For $Mg^{2+,}$ the highest rejection was 89.95% for the 4CG hydrogel membrane prepared at 9000 rpm. Overall, the results suggest that the centrifugal force significantly impacts the rejection of metal ions from aqueous solutions using centrifugal. The rejection of each metal ion may vary depending on the centrifugal speed and the concentration of AC in the CG hydrogel membrane. Therefore, selecting an appropriate centrifugal speed and CG type is essential based on the target metal ions in the feed solution. Generally, the best rejection of all ions was achieved at higher AC concentration and centrifugation speeds, and it was in the following order Pb^{2+}> Cu^{2+}> Mg^{2+}> Ca^{2+}.

The rejection of divalent ions by CG hydrogel membranes depends on many environmental and experimental factors such as the type and concentration of metal ions, the complexing ability of metal ions, ionic radius, ions hydration energy, hydrogel structure, the uptake time, and reactive sites available on the CG hydrogels' surface. These factors affect the interaction between the CG hydrogel membrane and divalent ions, hence, ions' rejection efficiency from solutions. For example, for all CG hydrogel membranes and centrifugation speeds, lead exhibited the highest rejection by the CG hydrogel membranes, followed by copper, magnesium, and calcium, with the lowest rejection. The ionic radius of Pb^{2+} is 121 p.m., significantly more significant than that of Cu^{2+} and Mg^{2+}, which are 80 p.m. and 72 p.m., indicating that Pb^{2+} has a smaller hydrated radius (401 p.m.), making it a stronger Lewis acid than other metals. As a result, Pb^{2+} has a higher attraction for the oxygenated groups found on the surface of AC, including carboxylic and phenolic groups, which are considered complex

Lewis bases. The electronegativity of Pb^{2+}, Cu^{2+}, and Mg^{2+} follows the sequence Pb^{2+} (2.3) > Cu^{2+} (1.9) > Mg^{2+} (1.3), supporting the idea that electrostatic forces drive the attraction between the metal ions and AC surface groups. Regarding the ion exchange mechanism, it is reasonable to anticipate that a metal with a higher electronegativity or acidity will exhibit greater reactivity with a protonated site compared to a metal with a lower electronegativity or acidity.

Figure 7 also revealed that the hydrogel membranes' rejections of divalent ions decreased with increasing the feed concentration from 10 mg/L to 1000 mg/L. The electrostatic charge screening of the hydrogel membranes resulted in low ion rejection at 1000 mg/L feed concentrations. The hydrogel membrane rejection can be attributed to the synergetic effects of different mechanisms [39]. The removal of heavy metals in CG hydrogel membranes can be attributed to two primary mechanisms: ion exchange and electrostatic attraction. These mechanisms play a crucial role in the adsorption and co-precipitation of heavy metal ions onto the surface of the CG hydrogel membrane. Ion Exchange: The CG hydrogel membranes possess ion exchange sites or functional groups that can undergo ion exchange with heavy metal ions present in the solution. These exchange sites, such as the carboxylate (-COO-) group, are typically negatively charged. Heavy metal ions, which are positively charged, can exchange ions with these sites. When the CG hydrogel membrane encounters a solution containing heavy metal ions, the positively charged metal ions are attracted to the negatively charged exchange sites on the membrane surface. This electrostatic attraction allows the metal ions to replace other ions bound to the exchange sites, resulting in the adsorption of heavy metals onto the membrane. Electrostatic Attraction: The negatively charged ions on the surface of the CG hydrogel membrane can also facilitate the adsorption process through electrostatic attraction. Heavy metal cations, being positively charged, are attracted to the negatively charged surface of the membrane. This electrostatic interaction between the metal cations and the negatively charged ions on the CG hydrogel surface enhances the adsorption of heavy metals. The attractive forces between opposite charges facilitate the binding of heavy metal ions to the membrane. Additionally, co-precipitation can occur because of ion exchange. When heavy metal ions exchange with ions on the CG hydrogel surface, they can form insoluble compounds or complexes. These insoluble compounds can then precipitate onto the membrane surface, leading to the co-precipitation of heavy metals. Combining ion exchange and electrostatic attraction in CG hydrogel membranes effectively removes heavy metal ions from solutions. The functional groups and negative charge on the membrane surface contribute to the adsorption and co-precipitation processes, enabling the efficient capture and removal of heavy metals. At a feed concentration of 1000 mg/L, the 4CG hydrogel membrane rejection of Mg^{2+}, Ca^{2+}, Pb^{2+}, and Cu^{2+} is 84, 30, 97, and 95% (**Figure 8**). Compared to the same 4CG hydrogels with a 10 mg/L feed concentration, the reduction of rejection of divalent ions decreased by 2.5% for Pb^{2+}, 5.5% for Mg^{2+}, 54.5% for Ca^{2+}, and 4.9% for Cu^{2+}. The rejection of the CG hydrogel to divalent ions is more significant for Cu^{2+} and Pb^{2+} than for Mg^{2+} and Ca^{2+}. It is attributed to the differences in these elements' chemical and physical properties like hydrate ions and electronegativity. The trend observed in this experiment is that increasing the concentration of AC in the aluminium hydroxide hydrogel improves its performance in removing ions from a solution. The results show that as the concentration of AC increases from 1 g/L to 4 g/L, the rejection for Ca^{2+}, Mg^{2+}, Cu^{2+}, and Pb^{2+} in a solution of 10 mg/L increases. Also, the rejection for these ions in a solution of 1000 mg/L increases with increased AC concentration. The trend also shows that the hydrogel performs better at removing Cu^{2+} and Pb^{2+} ions than Ca^{2+} and Mg^{2+} ions. As the concentration of ions in the solution increases, the rejection of the hydrogel membrane decreases, but this decrease tends to be less significant at higher AC concentrations.

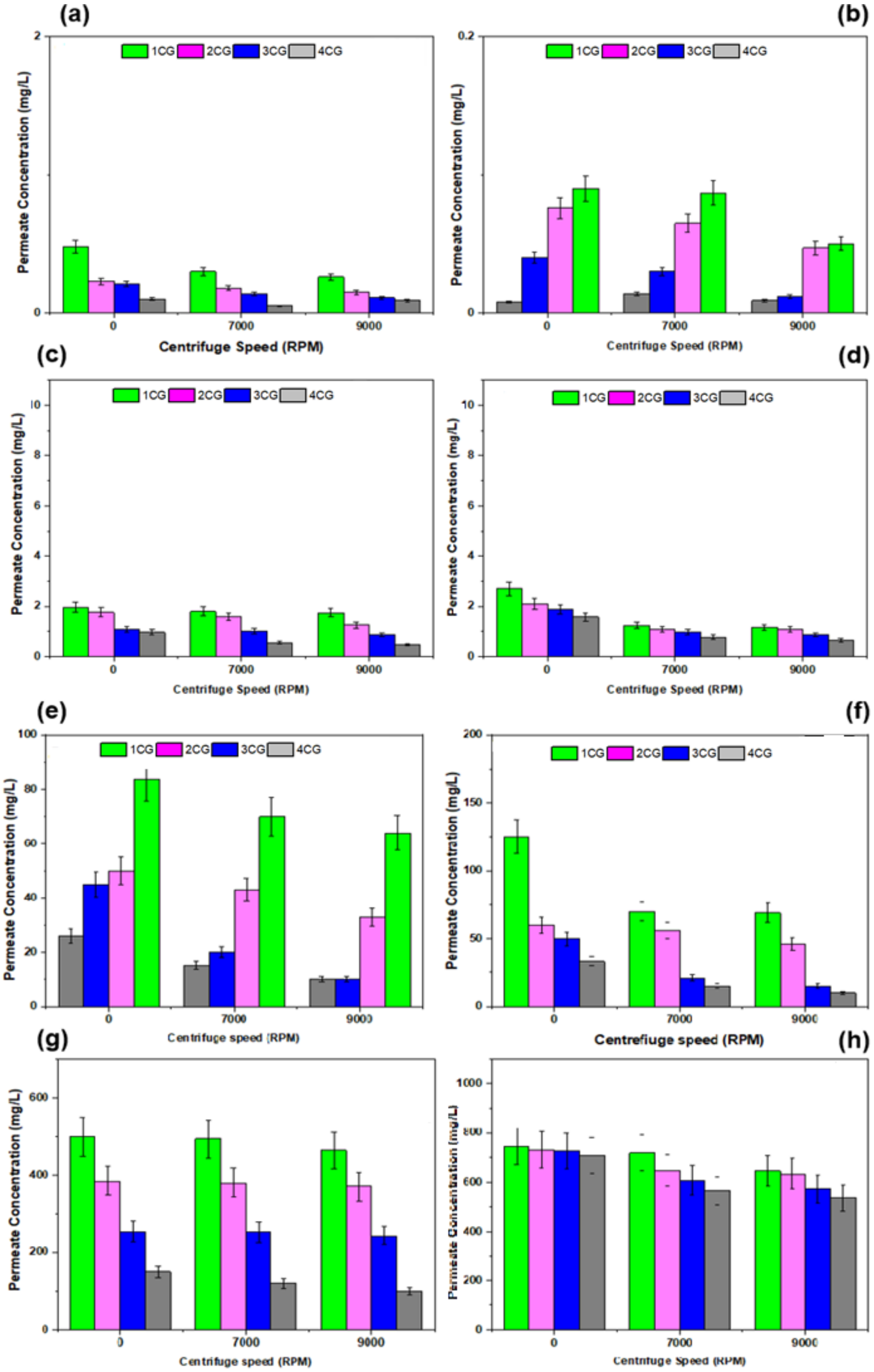

Figure 7*:* Removal metal ions at 10 mg/L& 1000 mg/l at different concentration of AC (a) 10 mg/L Pb (b) 10 mg/L Cu (c) 10 mg/L Mg (d) 10 mg/L Ca (e) 1000 mg/L of Pb (f)1000 mg/L Cu (g)1000 mg/L Mg(h) 1000 mg/L Ca

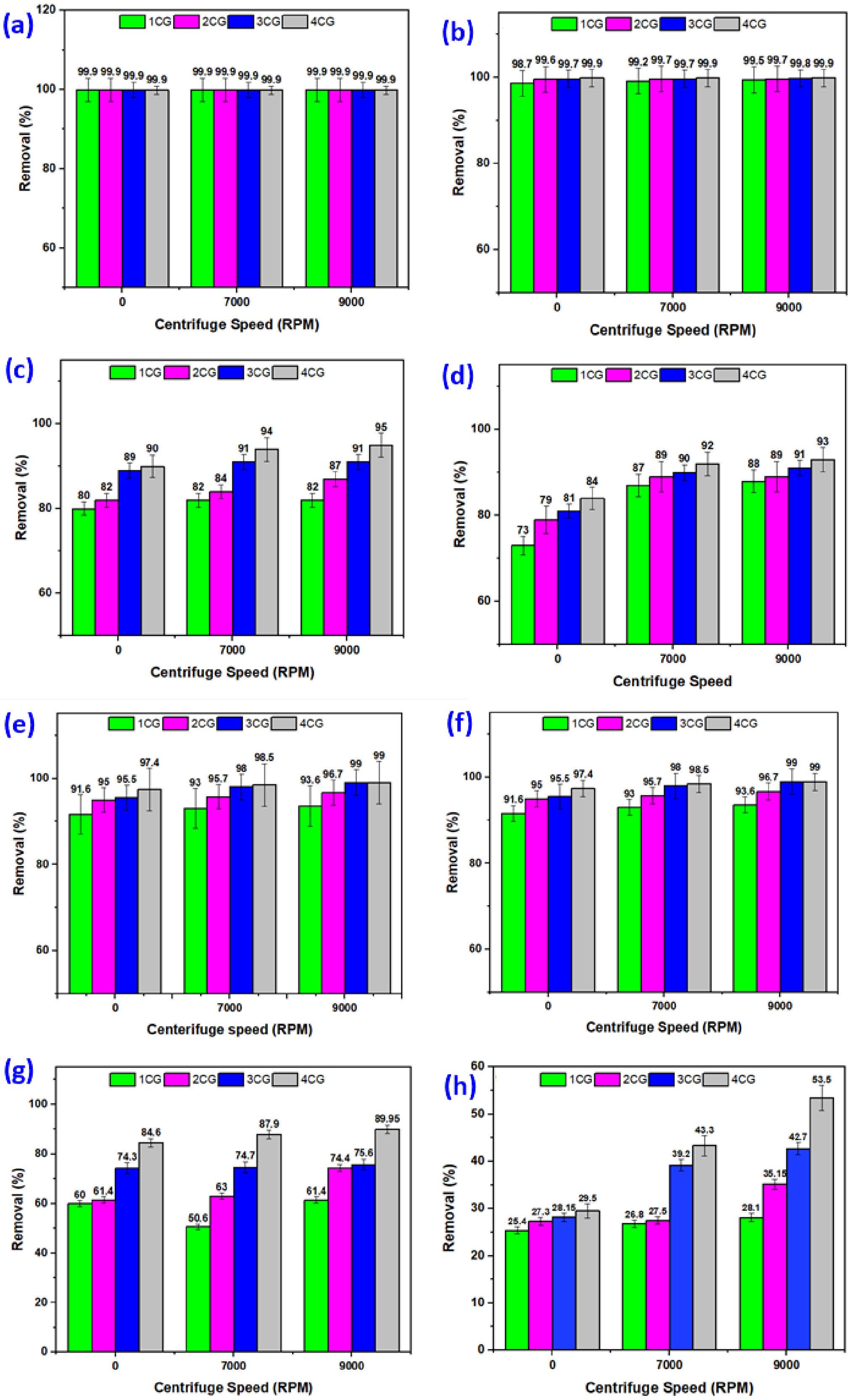

Figure 8*:* Removal percentage at 10 mg/L& 1000 mg/l at different concentration of AC (a) 10 mg/L Pb (b) 10 mg/L Cu (c) 10 mg/L Mg (d) 10 mg/L Ca (e) 1000 mg/L of Pb (f)1000 mg/L Cu (g)1000 mg/L Mg(h) 1000 mg/L Ca

3.3 Copper rejection in the filtration cycles

Four filtration cycles were conducted to investigate the Cu^{2+} ions rejection in consecutive cycles using a 10 mg/L feed concentration (**Figure 9**). A 4CG hydrogel without centrifugation was used in the tests because of its high-water flux and the trivial impact of the centrifugation process on Cu^{2+} ions rejection by the CG (**Figure 8**).

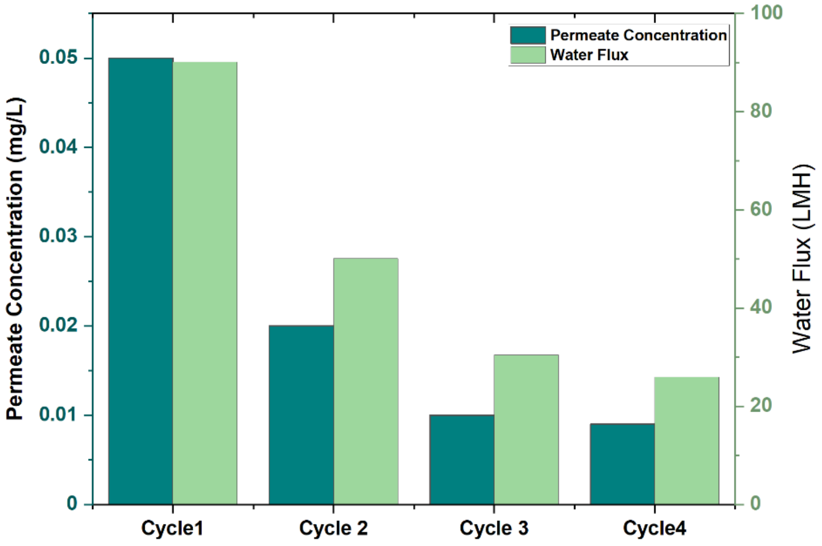

Figure 9: Reusability of 4 CG in four cycles with copper sulfate in 10 mg/L and water flux in 4 cycles at room temperature

The 4CG hydrogel membrane was put on a fabric material and left for a few minutes to settle down before conducting the filtration tests. Experimental results revealed that the water flux declined through the consecutive filtration cycles, and it was 95 LMH in the first cycle, 50.1 LMH in the second cycle, 30.5 LMH in the third cycle, and 26.01 LMH in the fourth cycle. The water flux in the first filtration cycle was roughly two times that in the third filtration cycle, and it could be due to a reduction in CG's pore size, resulting in a dramatic drop in water flux. The feed concentration of Cu2+ was 10 mg/L and reduced to 0.008 mg/L in the synthetic water after the first filtration cycle. The 4CG hydrogel membrane was used in multiple filtration cycles, with more than 99% Cu2+ rejection after 4 cycles, as shown in Figure 9. The result indicates that the final concentration of Cu2+ ions in the first, second, third, and fourth filtration cycles was 0.005, 0.002, 0.001and 0.0009 mg/L, respectively. Indeed, the 4CG rejection of Cu2+ ions was not affected in the consecutive filtration cycles, in which the 4CG hydrogel membrane achieved over 99% rejection.

3.4 Landfill leachate wastewater treatment

The efficiency of the ion's rejection by the 4CG hydrogel membrane was evaluated using biologically treated landfill leachate. All experiments were performed three times under dead-end filtration mode conditions with a constant head of 10 cm (about 0.01 bar). Landfill leachate contains various heavy metals such as lead, chromium, arsenic, copper, nickel, zinc, and mercury at various concentrations **(Table 1).** Landfill leachate quality is typically evaluated based on parameters such as total organic carbon (TOC), pH, suspended solids (SS), heavy metal content, or turbidity, which indicate the leachate's quality.

Figure 10 displays heavy metal concentrations in the 4CG permeate after treatment. The heavy metals rejection by the 4CG hydrogel membrane was more than 90% for Ni, Zn, Pb, As, and Cu ions. The high rejection is attributed to the electrostatic of the 4CG hydrogel membrane, which attracts and removes positively charged ions such as heavy metals. The heavy metal ions in the leachate wastewater, mostly divalent or trivalent, are electrostatically attracted to the hydrogel membrane. The GC rejection of heavy metals increased in the following order As>Ni>Pb>Zn>Cu>Mn (**Figure 10**). Also, the hydrogel membrane is anticipated to have a higher rejection of ions with larger ionic radii, such as Ba. In other words, the hydrogel membrane will show a higher resistance level to divalent or large molecular weight ions rejected by size exclusion or electrostatic repulsion.

The study found that monovalent ions such as K^+ (99.73 mg/L) and Na^+ (1600 mg/L) were abundant, whereas multivalent ions such as Ca^{2+} (179.71 mg/L) and Mg^{2+} (81.69 mg/L) had lower concentrations in the feed solution. Furthermore, the 4CG hydrogel was not successful in removing monovalent ions. The CG hydrogel's rejection of Na^+ was only 10%, which can be attributed to its low electronegativity and the high concentration of other cations in the leachate. Ca^{2+} and Mg^{2+} ions exhibit different behaviour in the landfill leachate due to their high hydration-free energies. Ions have a weak attraction to water molecules, shed their hydration shells, and pass through the CG pores, resulting in a rejection. In contrast, ions that firmly retain water molecules in their hydration shells struggle to shed them and are thus retained by the hydrogel membrane. Conversely, ions with larger crystal radii, such as K^+ and Na^+, have weaker hydration shells, which allows them to separate from their hydration layer during adsorption by hydrogel materials (**Table 3)**.

Unlike reverse osmosis and nanofiltration processes, the CG hydrogel membrane does not generate brine wastewater since it operates in a dead-end filtration mode. The dead-end filtration captures metal ions in the feed solution for reuse. A solvent at proper pH would be used for metal ions recovery at the end of the filtration process.

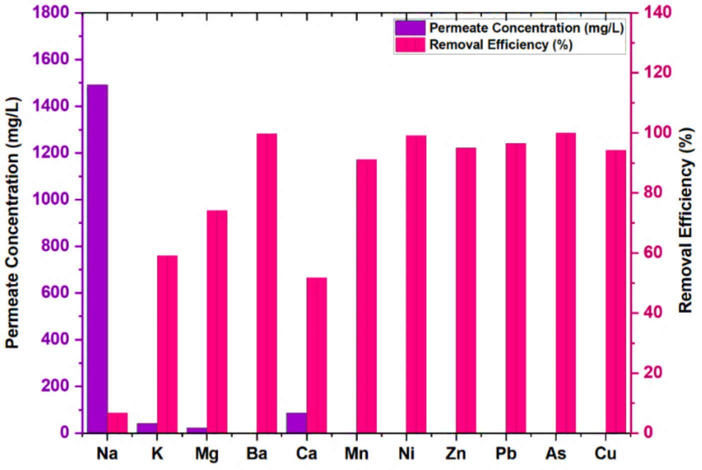

Figure 10: Concentrations and rejection of heavy metals after the CG hydrogel membrane treatment of leachate wastewater

The study also evaluated the removal of Total Organic Carbon (TOC) from landfill leachate. Experimental tests were conducted for 90 minutes, and samples were analyzed for their total organic carbon (TOC) content. CG effectively removed 53% of TOC from the landfill leachate. The study revealed that the TOC concentration in the CG permeate was 73.78 mg/L, and the CG hydrogel membrane effectively removed 53% of TOC from the landfill leachate.

Table 3- Metal ions, a respective group in the periodic table, ionic radii, hydration energy, and electronegativity

Ion	Ionic radii, nm	Electronegativity	Hydrated radii, nm	Hydration energy, $KJ \cdot mol^{-1}$
Na^+	0.102	0.9	0.358	-406
K^+	0.138	0.8	0.331	-322
Mg^{2+}	0.072	1.3	0.428	-1921
Ca^{2+}	0.100	1.0	0.412	-1577
Ba^{2+}	0.136	0.9	0.404	-1305
Mn^{2+}	0.067	1.5	-	-1841
Ni^{2+}	0.069	1.9	0.404	-2105
Pb^{2+}	0.202	2.3	0.401	-1480
Cu^{2+}	0.096	1.9	0.419	

4. Conclusions

This study demonstrated the feasibility of carbon-based hydrogel for water purification and wastewater treatment. The hydrogel rejection rate increased with the concentration of activated carbon from 1 g/L to 4 g/L. Furthermore, centrifugation can effectively enhance the rejection of heavy metals by hydrogel membrane. Key findings from this study are as follows:

1. The 4CG hydrogel membrane achieved the maximum rejection efficiency in the following order: $Pb^{2+} > Cu^{2+} > Mg^{2+} > Ca^{2+}$.
2. Water flux decreased with increased activated carbon from 1 g/L to 4 g/L due to pore volumes reduction in the hydrogel prepared with 4 g/L activated carbon. Nevertheless, the 4 CG hydrogel membrane exhibited the best ions rejection
3. The water flux of the CG hydrogel membranes decreases by increasing the centrifugation speed or the activated carbon concentration, whereas the membrane's rejection of ions increases.
4. Multivalent ions remain removed due to compensation for decreased electrostatic repulsion. A 4CG hydrogel membrane charge has higher ionic strength, but the more permeable monovalent co-ions pass through the 4CG more easily, balancing the effect.

The CG hydrogel membrane could be designed to achieve higher water flux or ion rejection based on the feed solution characteristics. The findings of this study have important implications for developing sustainable water treatment strategies and protecting aquatic ecosystems and human health. Based on the above results, CG exhibited better performance in ion separation. It can be concluded that CG has strong potential as an economical alternative adsorbent material for heavy metal rejection.

Credit authors statement

Elika Karbassiyazdi: Conceptualization, methodology, formal analysis, visualization, data curation, writing-original draft, investigation, writing & editing. Ali Altaee: Supervision, conceptualization, methodology, formal analysis, data curation, funding support, writing, investigation, review & editing. Ibrar Ibrar: data curation, review & editing. Amir Razmjou: Methodology, data curation, formal analysis, review & editing. Namuun Ganbat: Review and editing. Ali Malekizadeh: review and editing. Romina Ghobadi: review & editing. Hadi Khabbaz: Supervision, formal analysis, review & editing.

Acknowledgements

Elika Karbassiyazdi is grateful for the financial support from the Australian Training and Research Scholarship for her PhD studies.

Reference

1. Men, C., et al., *Pollution characteristics, risk assessment, and source apportionment of heavy metals in road dust in Beijing, China.* Science of The Total Environment, 2018. **612**: p. 138-147.
2. Alqadami, A.A., et al., *Efficient removal of toxic metal ions from wastewater using a recyclable nanocomposite: A study of adsorption parameters and interaction mechanism.* Journal of Cleaner Production, 2017. **156**: p. 426-436.
3. Perumal, S., et al., *A Short Review on Recent Advances of Hydrogel-Based Adsorbents for Heavy Metal Ions.* Metals, 2021. **11**(6): p. 864.
4. Karbassiyazdi, E., et al., *A juxtaposed review on adsorptive removal of PFAS by metal-organic frameworks (MOFs) with carbon-based materials, ion exchange resins, and polymer adsorbents.* Chemosphere, 2023. **311**: p. 136933.
5. Obotey Ezugbe, E. and S. Rathilal, *Membrane Technologies in Wastewater Treatment: A Review.* Membranes, 2020. **10**(5): p. 89.
6. Benvenuti, T., et al., *Closing the loop in the electroplating industry by electrodialysis.* Journal of Cleaner Production, 2017. **155**: p. 130-138.
7. Shahrokhi-Shahraki, R., et al., *High efficiency removal of heavy metals using tire-derived activated carbon vs commercial activated carbon: Insights into the adsorption mechanisms.* Chemosphere, 2021. **264**: p. 128455.
8. Lin, Z., et al., *Preparation of Chitosan/Calcium Alginate/Bentonite Composite Hydrogel and Its Heavy Metal Ions Adsorption Properties.* Polymers, 2021. **13**(11): p. 1891.
9. Godiya, C.B., et al., *Carboxymethyl cellulose/polyacrylamide composite hydrogel for cascaded treatment/reuse of heavy metal ions in wastewater.* Journal of Hazardous Materials, 2019. **364**: p. 28-38.
10. Godiya, C.B., et al., *Amine-bilayer-functionalized cellulose-chitosan composite hydrogel for the efficient uptake of hazardous metal cations and catalysis in polluted water.* Journal of Hazardous Materials, 2022. **436**: p. 129112.
11. Moon, C.-J. and J.-h. Lee, *Use of curdlan and activated carbon composed adsorbents for heavy metal removal.* Process Biochemistry, 2005. **40**(3): p. 1279-1283.
12. Perumal, S., et al., *Graphene oxide-embedded chitosan/gelatin hydrogel particles for the adsorptions of multiple heavy metal ions.* Journal of Materials Science, 2020. **55**(22): p. 9354-9363.
13. Queiroz, L.S., et al., *Activated carbon obtained from amazonian biomass tailings (acai seed): Modification, characterization, and use for removal of metal ions from water.* Journal of Environmental Management, 2020. **270**: p. 110868.
14. Wahlström, N., et al., *Ulvan dialdehyde-gelatin hydrogels for removal of heavy metals and methylene blue from aqueous solution.* Carbohydrate Polymers, 2020. **249**: p. 116841.

15. Yang, S.C., et al., *Mesoporous cellulose-chitosan composite hydrogel fabricated via the co-dissolution-regeneration process as biosorbent of heavy metals.* Environmental Pollution, 2021. **286**: p. 117324.
16. Tirtom, V.N. and A. Dinçer, *Effective removal of heavy metals from an aqueous solution with poly(N-vinylimidazole-acrylamide) hydrogels.* Separation Science and Technology, 2021. **56**(5): p. 912-924.
17. Chang, H., et al., *State-of-the-art insights on applications of hydrogel membranes in water and wastewater treatment.* Separation and Purification Technology, 2023. **308**: p. 122948.
18. Bai, Z., et al., *A Solvent Regulated Hydrogen Bond Crosslinking Strategy to Prepare Robust Hydrogel Paint for Oil/Water Separation.* Advanced Functional Materials, 2021. **31**(49): p. 2104701.
19. Xie, W., et al., *Charge-Gradient Hydrogels Enable Direct Zero Liquid Discharge for Hypersaline Wastewater Management.* Advanced Materials, 2021. **33**(24): p. 2100141.
20. Shi, Y., et al., *All-day fresh water harvesting by microstructured hydrogel membranes.* Nature Communications, 2021. **12**(1): p. 2797.
21. Zhang, Y., et al., *Polypropylene non-woven supported calcium alginate hydrogel filtration membrane for efficient separation of dye/salt at low salt concentration.* Desalination, 2021. **500**: p. 114845.
22. Marks, R., et al., *Catalytic Hydrogel Membrane Reactor for Treatment of Aqueous Contaminants.* Environmental Science & Technology, 2019. **53**(11): p. 6492-6500.
23. Yazdi, M.K., et al., *Hydrogel membranes: A review.* Materials Science and Engineering: C, 2020. **114**: p. 111023.
24. Ao, C., et al., *Reusable, salt-tolerant and superhydrophilic cellulose hydrogel-coated mesh for efficient gravity-driven oil/water separation.* Chemical Engineering Journal, 2018. **338**: p. 271-277.
25. Li, X., et al., *3D printed robust superhydrophilic and underwater superoleophobic composite membrane for high efficient oil/water separation.* Separation and Purification Technology, 2020. **237**: p. 116324.
26. Zhang, W., H. Huang, and R. Bernstein, *Zwitterionic hydrogel modified reduced graphene oxide/ZnO nanocomposite blended membrane with high antifouling and antibiofouling performances.* Journal of Colloid and Interface Science, 2022. **613**: p. 426-434.
27. Zhang, D., et al., *Scalable, Flexible, Durable, and Salt-Tolerant CuS/Bacterial Cellulose Gel Membranes for Efficient Interfacial Solar Evaporation.* ACS Sustainable Chemistry & Engineering, 2020. **8**(24): p. 9017-9026.
28. Lu, M. and H. Zhang, *Preparation and decontamination performance of a flexible self-standing hydrogel photocatalytic membrane.* Journal of Membrane Science, 2022. **644**: p. 119979.
29. Hu, X., et al., *Self-assembly of binary oppositely charged polysaccharides into polyelectrolyte complex hydrogel film for facile and efficient Pb2+ removal.* Chemical Engineering Journal, 2020. **388**: p. 124189.
30. Baruah, U., A. Konwar, and D. Chowdhury, *A sulphonated carbon dot–chitosan hybrid hydrogel nanocomposite as an efficient ion-exchange film for Ca2+ and Mg2+ removal.* Nanoscale, 2016. **8**(16): p. 8542-8546.
31. Abdulrazak, S., K. Hussaini, and H.M. Sani, *Evaluation of removal efficiency of heavy metals by low-cost activated carbon prepared from African palm fruit.* Applied Water Science, 2017. **7**(6): p. 3151-3155.
32. Ji, D. and J. Kim, *Recent Strategies for Strengthening and Stiffening Tough Hydrogels.* Advanced NanoBiomed Research, 2021. **1**(8): p. 2100026.
33. Coleman, J.N., U. Khan, and Y.K. Gun'ko, *Mechanical Reinforcement of Polymers Using Carbon Nanotubes.* Advanced Materials, 2006. **18**(6): p. 689-706.
34. Wang, S.-F., et al., *Preparation and Mechanical Properties of Chitosan/Carbon Nanotubes Composites.* Biomacromolecules, 2005. **6**(6): p. 3067-3072.
35. Hosseinzadeh, H., *Synthesis of carrageenan/multi-walled carbon nanotube hybrid hydrogel nanocomposite for adsorption of crystal violet from aqueous solution.* Polish Journal of Chemical Technology, 2015. **17**(2): p. 70-76.
36. Uzoma, K.C., et al., *Influence of biochar application on sandy soil hydraulic properties and*

nutrient retention. Journal of Food Agriculture & Environment, 2011. **9**: p. 1137-1143.

37. Saghandali, F., M. Baghban Salehi, and V. Taghikhani, *Hydrogel nanocomposite network elasticity parameters as a function of swelling ratio: from micro to macro flooding.* Journal of Industrial and Engineering Chemistry, 2023.
38. Salehi, M.B. and A.M. Moghadam, *Chapter 2 - Sustainable production of hydrogels*, in *Sustainable Hydrogels*, S. Thomas, et al., Editors. 2023, Elsevier. p. 23-46.
39. Yadav, S., et al., *Surface modification of nanofiltration membrane with kappa-carrageenan/graphene oxide for leachate wastewater treatment.* Journal of Membrane Science, 2022. **659**: p. 120776.

Supplementary information S.1

Evaluating the Performance of Carbon-Based Hydrogel Membrane for Ion Separation in Synthetic and Landfill Leachate

Elika Karbassiyazdi[a], Ali Altaee[a] , Ibrar Ibrar[a], Amir Razmjou[b], Namuun Ganbat[a], Ali Malekizadeh[a], Romina Ghobadi [a], Hadi Khabbaz [a],

[a] Center for Green Technology, School of Civil and Environmental Engineering, University of Technology Sydney, 15 Broadway, NSW 2007, Australia

[b] Mineral Recovery Research Center (MRRC), School of Engineering, Edith Cowan University, Joondalup, Perth, WA, 6027, Australia

[*]Corresponding author Email address: ali.altaee@uts.edu.au

Table S1, BET Analysis of different hydrogel membranes

Sample	Pore volume	Surface area
HG	0.076 cc/g	25.731 m^2/g
1 CG	0.195 cc/g	106.536 m^2/g
2 CG	0.268 cc/g	223.066 m^2/g
3 CG	0.70 cc/g	342.248
4 CG	1.644 cc/g	756.919 m2/g

S.1. FT-IR Analysis

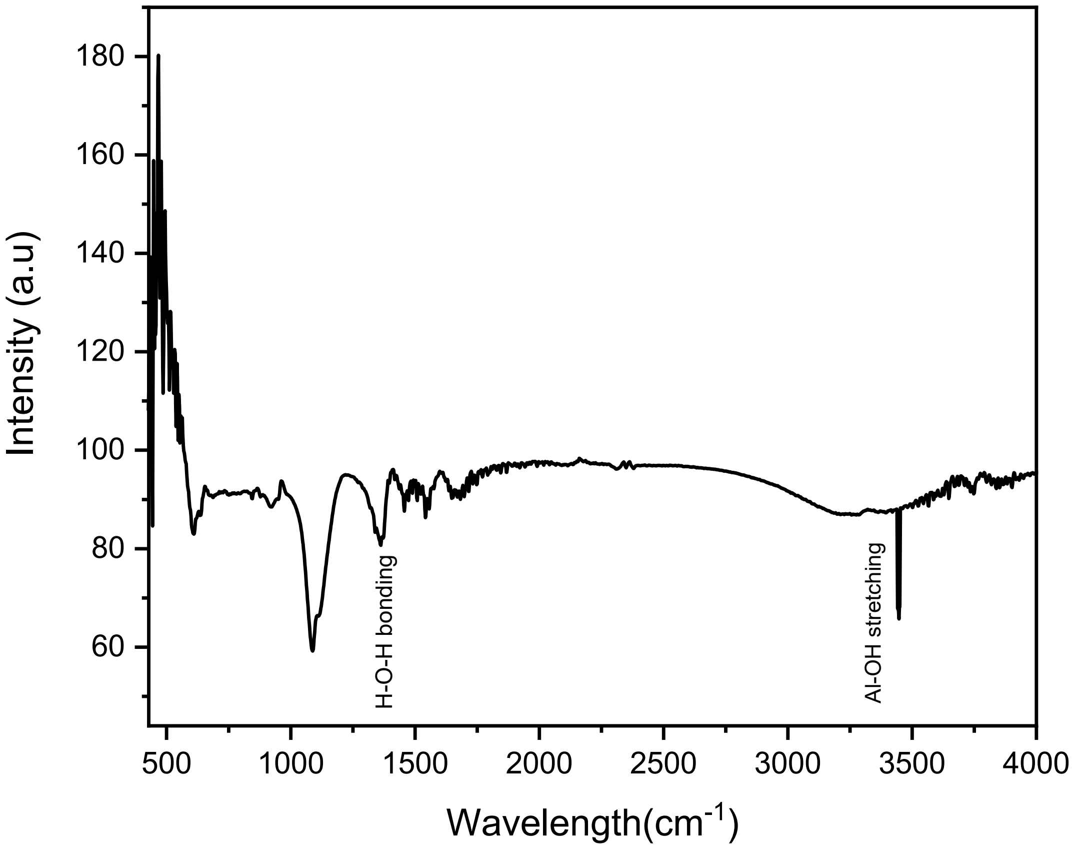

Figure S.1. FT-IR analysis of CG

S.2. EDX analysis

The EDX analysis were imported from the SEM system directly and are presented in Figure S2 for all the hydrogels.

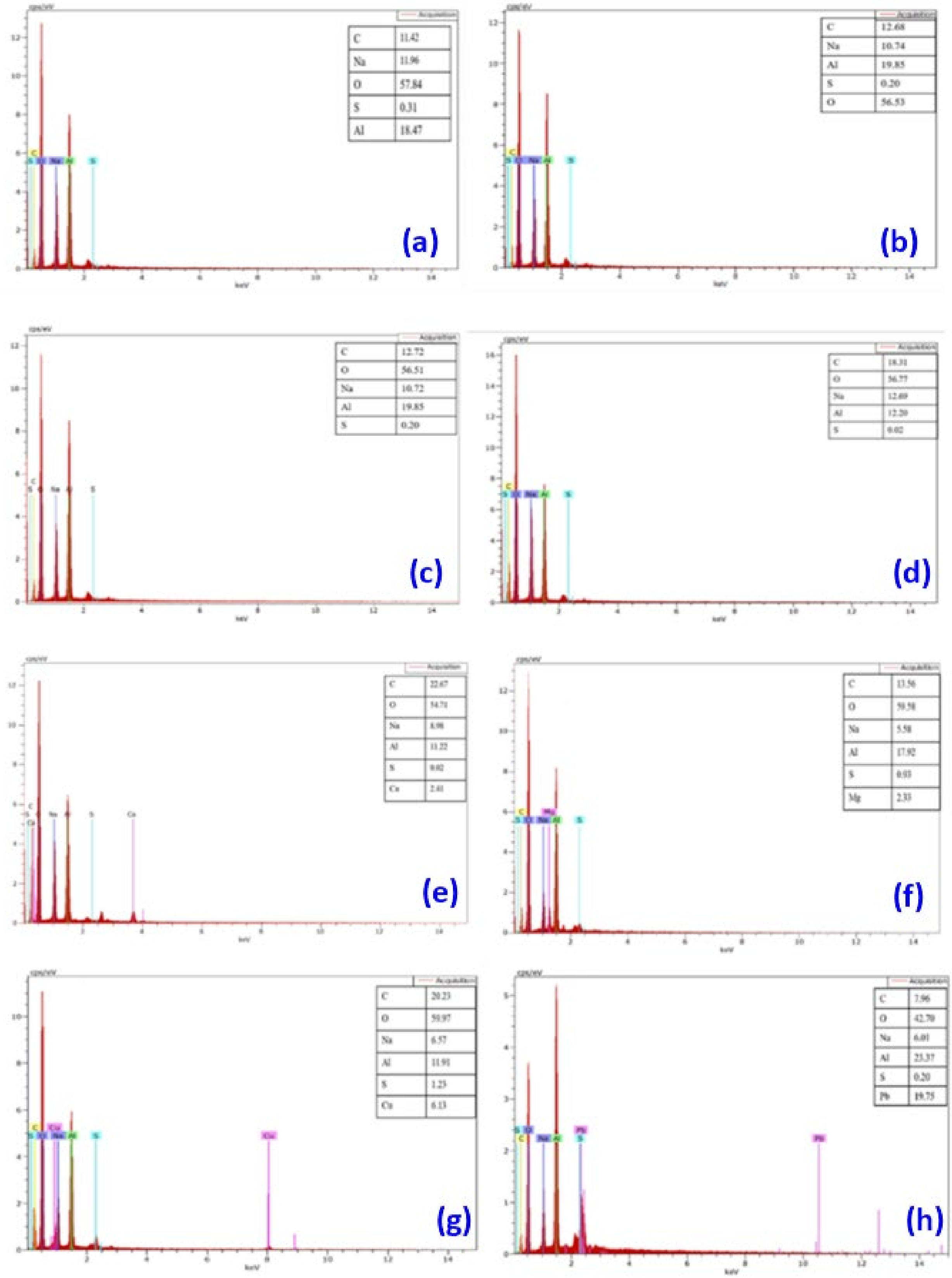
(a)
C 11.42
Na 11.96
O 57.84
S 0.31
Al 18.47
(b)
C 12.68
Na 10.74
Al 19.85
S 0.20
O 56.53
(c)
C 12.72
O 56.51
Na 10.72
Al 19.85
S 0.20
(d)
C 18.31
O 56.77
Na 12.69
Al 12.20
S 0.02
(e)
C 22.67
O 54.71
Na 8.98
Al 11.22
S 0.02
Ca 2.41
(f)
C 13.56
O 59.58
Na 5.58
Al 17.92
S 0.53
Mg 2.33
(g)
C 20.23
O 59.97
Na 6.57
Al 11.91
S 1.23
Cu 6.13
(h)
C 7.96
O 42.70
Na 6.01
Al 23.37
S 0.20
Pb 19.75
cps/eV
keV
Acquisition

Figure S2: Energy Dispersive X-ray Spectroscopy (EDS) **(a)** 1CG before treatment **(b)** 2CG **(c)** 3CG **(d)** 4 CG **(e)** 4CG after treatment loaded 1000 mg/L Ca **(e)** 4CG after treatment loaded1000 mg/L Mg **(f)** 4CG loaded 1000 mg/L Cu **(g)** 4CG after treatment loaded 1000 mg/L Pb in room temperature